Hydrogen Concentration, States and Distribution in Magnesium and Its Alloys at Stress Corrosion Cracking

Evgeniy Merson[1*], Pavel Myagkikh[1], Vitaliy Poluyanov[1], Dmitri Merson[1], Alexei Vinogradov[2]

[1]*Institute of Advanced Technologies, Togliatti State University, Belorusskaya str. 14, Togliatti 445667, Russian Federation*

[2]*Department of Mechanical and Industrial Engineering, Norwegian University of Science and Technology – NTNU, N-7491 Trondheim, Norway*

**Email: mersoned@gmail.com*

Abstract

One of the main challenges impeding wider uptake of magnesium alloys by the industry is their poor resistance to general corrosion and stress-corrosion cracking (SCC), the nature of which is not fully understood. Although SCC is generally associated with hydrogen embrittlement, the experimental data on the possible hydrogen state, concentration and distribution in Mg is scarce, and its role in SCC is unclear. These issues are addressed in the present study using as-cast technically pure Mg as well as wrought ZK60 and AZ31 alloys slow-strain rate tensile tested in air and in corrosive media before and after prestraining. Hydrogen concentration and extraction curves have been obtained and analyzed for the specimens tested in corrosive media. It is found that most part of hydrogen is contained in the corrosion products while the concentration of diffusible hydrogen in the matrix is negligible for all the materials studied. On the basis of fractographic observations combined with gas-analysis and mechanical testing data, it is suggested that SCC of the ZK60 and AZ31 alloys results from brittle cracking of a surface hydride film, while SCC of pure Mg is likely associated with adsorbed hydrogen facilitating ductile fracture.

1. Introduction.

A steadily growing interest in the development of wrought magnesium alloys as structural materials for engineering and bio-medical applications has been seen since the 2000s. The main challenges impeding wider uptake of magnesium alloys by the industry, besides low plastic deformation ability, are associated with their low resistance to general corrosion, and particularly to stress-corrosion cracking (SCC) [1–3], which is actually even more harmful. Nevertheless, the

understanding of the nature of this phenomenon in relation to magnesium is currently insufficient.

The SCC of Mg alloys readily occurs in NaCl [4,5], $NaSO_4$ [6,7] and many other aqueous solutions including distilled water. Under normal conditions, the surface of magnesium is covered with a thin layer of Mg oxide and hydroxide preventing corrosion of the base metal. The aggressive anions such as chloride or sulfate cause breakdown of the protective $Mg(OH)_2$ film providing access of corrosion environment to the juvenile Mg surface [8]. This triggers the anodic dissolution (AD) process, which is accompanied by the evolution of hydrogen adsorbing on the magnesium's surface or removing back to the environment in the form of gas. It has been argued that AD itself can be responsible for SCC. For example, in Mg-Al alloys, intergranular fracture occurs due to the preferential galvanic dissolution of the Mg matrix surrounding the β-phase particles, precipitating primarily along the grain boundaries [9]. However, the vast majority of existing findings indicate the importance of hydrogen embrittlement (HE) in the SCC mechanism [2,8,10]. There is a strong belief that atomic hydrogen adsorbed on the metal surface penetrates into the Mg matrix and somehow assists the crack-growth process, which is referred to as hydrogen-assisted cracking (HAC). However, the exact role of hydrogen in the HE mechanism in magnesium alloys has yet to be understood.

Several mechanisms have been proposed or adopted from the theories of HE of steels and other materials to explain the HAC phenomenon in magnesium and its alloys [2,8]. Some authors suggested that SCC of Mg alloys occurs by delayed hydride cracking (DHC) mechanism [4,11–14], in which crack propagation occurs by alternating formation and brittle fracture of magnesium hydrides ahead of the crack tip. According to the adsorption-induced dislocation emission (AIDE) model proposed by Lynch and Trevena [15], hydrogen adsorbed at the crack surface in pure Mg enhances dislocation emission from the crack tip, promoting extremely high velocities of ductile crack growth. The hydrogen-enhanced decohesion (HEDE) mechanism is associated with atomic hydrogen absorbed by the metal which weakens interatomic bonds and thus reduces the threshold stress of brittle cleavage cracking [8]. The theory of hydrogen-enhanced localized plasticity (HELP) implies that HAC occurs due to increased dislocations mobility, induced by the action of dissolved atomic hydrogen, interacting with dislocations ahead of the crack tip [16,17]. As follows from these features as well as from the detailed, dedicated reviews provided elsewhere [8,16–18], the DHC, HEDE and HELP mechanisms require hydrogen absorbed inside a metal while for the AIDE mechanism the only adsorbed hydrogen is needed. Besides, if the HEDE or HELP (or both) operate during SCC, it is reasonable to expect an appreciable concentration of diffusible hydrogen inside the metal. On the other hand, DHC implies the presence of hydrides. Thereby, the better insight into the hydrogen

states, its distribution and concentration is pivotal for understanding the HE mechanisms in metals. For Mg and its alloys, the existing data is quite scarce and sometimes controversial.

The presence of MgH_2 hydride forming the surface film and sitting in the corrosion products has been observed in pure Mg and its alloys subjected to corrosion or SCC. Chen et al. [6] using a blend of methods including the secondary ion mass-spectroscopy (SIMS) found that immersion or cathodic charging in 0.1 M Na_2SO_4 solution resulted in the formation of the magnesium hydride in the β-phase precipitating along the grain boundaries in the AZ91 alloy. It was concluded that the fracture of these brittle hydrides was responsible for the appearance of intergranular cracks. In contrast, Tuchscheerer and Krüger [5] did not find the X-Ray diffraction (XRD) peaks corresponding to hydrides in AZ31 immersed in distilled water for 14 days, although the SCC did occur. With the aid from SIMS, Zhou et al. [14] and Chen et al. [6] found segregations of hydrogen around crack tips. However, it is not clear whether the hydrogen was in the diffusible form or in the form of hydride.

Few studies provide information about the influence of SCC and corrosion on the concentration of hydrogen in Mg and its alloys. Using the inert gas fusion method, Chakrapani and Pugh [4] found that 24 h exposure of Mg-7.5Al alloy in NaC1-K_2CrO_4 solution resulted in the increase of hydrogen concentration up to 170 ppm. The subsequent vacuum annealing of corroded specimens at 385 °C during 24 h provided a reduction of hydrogen concentration down to 50 ppm, and just a slight recovery of mechanical properties. Morozova [19] reported the 3-4 fold increase in the hydrogen concentration (from about 20 up to 150 ppm) in MG90, Mg95 and ML5 alloys in humid air. Both these reports did not mention whether the corrosion products were removed from the specimens before the gas-analysis or not. Decomposition of corrosion products accompanying by hydrogen evolution during gas-analysis at elevated temperatures as well as during annealing could substantially affect the obtained hydrogen concentration values. For example, the hydrogen concentration was found to be in the range of 12-18 ppm after removing corrosion products from the ZK60 specimens slow-strain rate tensile (SSRT) tested in the 0.1%NaCl + 0.05%Na_2SO_4 + 0.05%$CaCl_2$ solution [14]. Although the authors used the carrier-gas hot extraction technique enabling the measurement of the concentration of diffusible hydrogen, neither the analysis regime including heating rate and temperature, nor the extraction curves have been provided, unfortunately. Thus, the actual amount of hydrogen absorbed by Mg and its alloys matrix during corrosion or SCC is still questionable. More specifically and very importantly is that the fraction of diffusible hydrogen capable to cause HAC is also unknown.

In the present study, by using the carrier-gas hot extraction method, we endeavor to address the above-highlighted issues related to the hydrogen states, concentration and distribution of hydrogen in pure Mg and its alloys subjected to SCC and corrosion.

2. Experimental

2.1. Materials and specimens

As-cast technically pure Mg, as well as commercially available extruded ZK60 and hot-rolled AZ31 alloys (MA14 and MA2-1 in Russian designation), were used in the present study. Chemical compositions of the materials were evaluated by the optical emission spectrometer ARL 4460 (Thermo Fisher Scientific) and are represented in Table 1. The round, threaded, 120 mm long specimens with the gauge part of 30 mm length and 6 mm diameter were machined along the rolling or extrusion direction.

Table 1 – Chemical composition of the alloys (in wt. %)

Material	**Mg**	**Al**	**Zn**	**Ca**	**Zr**	**Fe**	**Cu**	**Mn**	**Ce**	**Nd**	**Si**
ZK60		0.002	5.417	0.0004	0.471	0.001	0.002	0.005	0.002	0.003	0.003
AZ31	Balance	4.473	0.887	0.0015	-	0.002	0.003	0.312	0.017	0.007	0.008
Pure Mg		0.005	-	0.0002	-	0.067	-	0.002	0.009	0.001	0.003

To evaluate the effect of pre-strain on the hydrogen behavior, several ZK60, AZ31 and pure Mg specimens were plastically deformed to 4, 11 and 2% tensile strain, respectively, at 1 mm/min crosshead velocity. The extensometer was attached to the specimen surface to measure axial elongations. After unloading, these specimens were used for further slow strain rate tensile tests in a corrosive environment.

2.2. Slow strain rate tensile (SSRT) tests

SSRT testing was performed on a screw-driven testing frame in the air or in the aqueous 5g/l NaCl + 5g/l $K_2Cr_2O_7$ solution at the strain rate $5 \cdot 10^{-6}$ s^{-1} at room temperature.

After fracture, the specimens gauge part was mechanically cut into two pieces, one of which was immediately subjected to the hydrogen concentration analysis while the other was stored in liquid nitrogen to avoid diffusible hydrogen loss. The time lag between the end of the SSRT test and the beginning of the first gas-analysis did not exceed 10 minutes. Upon completion of the gas analysis, the second piece was removed from liquid nitrogen storage and immersed into the standard 20% CrO_3+ 1%$AgNO_3$ aqueous solution for 1 min to remove corrosion products from the specimen's surface. It was found that the weight loss of the not-corroded Mg specimens due to this procedure was lower than the measurement limit of the balance, i.e. <0.007%. This roughly corresponds to the surface layer of less than 15 nm thickness

for the given specimen geometry. As soon as the corrosion products were removed, the sample was subjected to the gas-analysis. All specimens were degreased in CCl_4 before gas-analysis.

2.3. Gas-analysis

In the present study, the carrier gas hot-extraction method implemented in the G8 (Bruker) gas-analyzer was used for determination of the hydrogen concentration in the Mg-based specimens. In this method, the sample inserted in the analytical quartz tube purging by an inert gas is heated up to the target temperature with the optional holding at the same temperature. Hydrogen extracted from the sample during heating was carried by the inert gas to the thermal conductivity detector (TCD). The concentration of extracted hydrogen was determined by the difference between thermal conductivities of pure carrier gas and the gas mixture containing extracted hydrogen. The gas-analyzer was calibrated by the standard steel samples with the known hydrogen concentration. This procedure is conducted by melt extraction where the sample is melted in the graphite crucible in the inert gas flux.

Preliminary tests showed that Mg partially evaporates and reacts with analytical quarts tube at the temperature above 450 °C. Thus, the target temperature was limited to 450 °C, and the steel substrate was used for the tests. The constant heating rate of 38 °C/min was set to heat the sample from 25 to 450 °C. Since hydrogen continued extracting at the target temperature, the sample was additionally held at this temperature for 600 s. For correct determination of the background level of the signal from the TCD at the end of the test, the heater was turned off for 600 s, and the hydrogen desorption rate dropped down to the background level. The 99.999% purity nitrogen was used as the carrier gas in the present tests. No significant reaction of nitrogen with Mg was observed at the temperatures used in the present study. The full cycle of the gas analysis included three steps: (1) heating from 25 to 450 °C during 675 s, (2) exposure at 450 °C during 600 s, (3) free cooling in nitrogen flux during 600 s

2.4. Microstructure and fracture surface characterization

Fractographic, metallographic and side surface examinations have been performed with the use of the confocal laser scanning microscope (CLSM) LEXT OLS4000 (Olympus) and the scanning electron microscope (SEM) SIGMA (Zeiss) equipped with the EDAX/TSL detector and the software package for the electron-backscattered diffraction (EBSD) analysis.

3. Results

3.1. Microstructure

Metallographic examination showed that the alloy ZK60 exhibits a fine grain structure having of 3 μm average grain diameter and numerous secondary phase particles, c.f. Fig. 1a, d. The microstructure of the hot-rolled alloy AZ31, Fig. 1b, e, is represented by equiaxial grains of 10 μm average diameter with second phase particles precipitated predominantly along grain boundaries. Pure Mg has a coarse grain structure with the grain diameter up to a few millimeters, c.f. Fig. 1c.

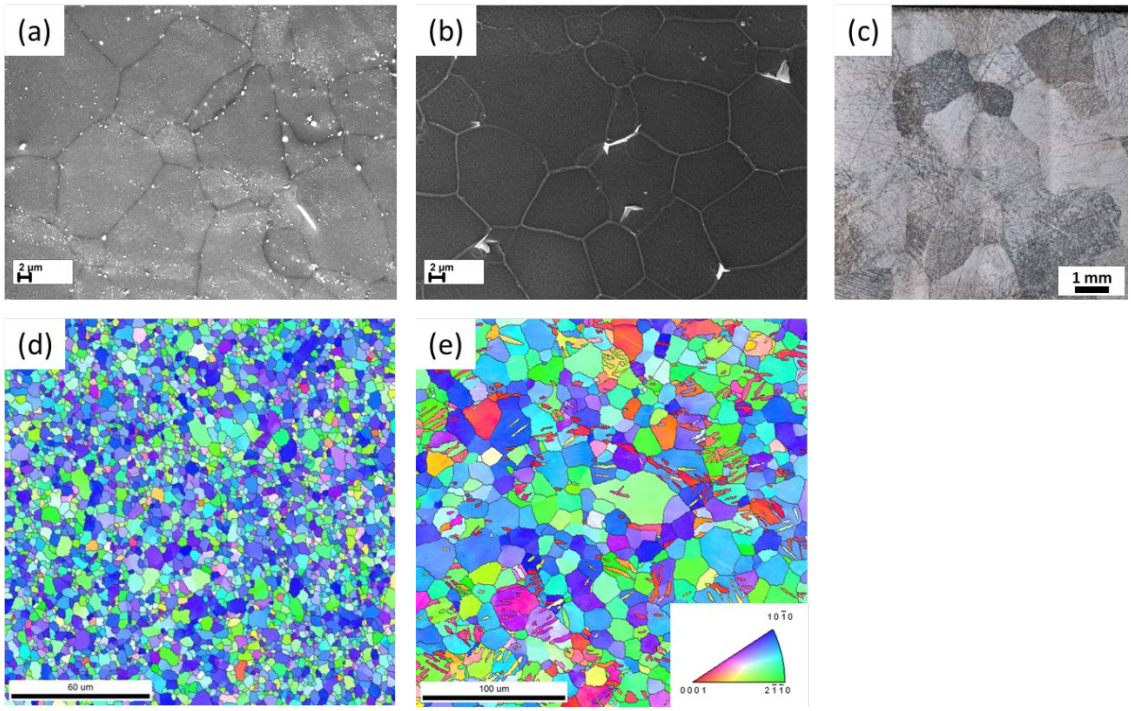

Fig. 1 – SEM (a, b), CLSM (c) and IPF (inverse pole figure colored) EBSD (d, e) images of the microstructure of ZK60 (a, d), AZ31 (b, e) and as-cast pure magnesium (c).

3.2. Slow strain rate tensile tests

When tested in air, all materials exhibit appreciable elongation, Table 2, though with the notably different strain hardening behavior. As follows from Fig. 2, the alloys AZ31 and ZK60 demonstrate pronounced strain hardening and the necking stages on the stress-strain diagrams, while pure magnesium fractures without necking. Among the investigated materials, the alloy ZK60 exhibits the higher yield stress and the ultimate tensile strength, while its uniform elongation is relatively short (of 7%), and the resistance to the localized deformation in the neck is relatively high, giving rise to the total elongation of 25%. Having approximately the same

elongation to failure and just a slightly smaller ultimate strength, the alloy AZ31 shows the considerably longer uniform elongation (in excess of 20%), lower yield stress and slower strain hardening rate at the onset of yielding. Pure Mg possesses a much lower strength and ductility than the alloys. As follows from Table 2 and Fig. 2 summarizing the mechanical properties of tensile tested alloys, both strength and ductility are reduced dramatically when the specimens were tested in corrosive media. Fracture of both alloys in the corrosive environment always occurs in the pseudo-elastic region of the stress-strain diagram, Fig. 2a and b, and the uniform elongation effectively nullifies. The absolute value of the ultimate tensile strength in the corrosive solution is higher for the alloy ZK60. However, in terms of the ultimate tensile strength / yield stress ratio, the alloy AZ31 has a better resistance to SCC. It is interesting, that prestraining results in the slight increase of the elongation to failure for both alloys. In pure Mg, the SCC causes the decrease in the elongation to failure, yield stress and ultimate tensile strength. In contrast to the alloys, the fracture of pure Mg occurs after significant plastic deformation at the stress higher than the yield point, c.f. Fig. 2c. Thus, in terms of the yield stress ratio, pure Mg exhibits a much lower susceptibility to SCC than both alloys studied. After prestraining, the elongation to failure of pure Mg decreases but the stress value at fracture increases.

Table 2 – Mechanical properties of as-cast pure Mg, ZK60 and AZ31 alloys SSRT-tested in air and in corrosive media before and after prestraining.

Alloy	Testing conditions	Ultimate tensile strength (MPa)	Elongation to failure (%)	Ultimate tensile strength /yield stress (in air) ratio
ZK60	In air	296±1	28.3±2.1	1.2±0.1
	In corrosive media	157±20	2.2±0.3	0.7±0.1
	In corrosive media, after 4% prestrain	224±16	2.9±0.2	0.9±0.1
AZ31	In air	272±2	25.1±1.2	1.9±0.1
	In corrosive media	129±11	2.6±0.1	0,9±0.1
	In corrosive media, after 11% prestrain	145±6	2.7±0.1	1±0.1
As-cast pure Mg	In air	55±6	6.9±0.1	3.7±0.2
	In corrosive media	26±3	5.6±0.3	1.7±0.1
	In corrosive media, after 2% prestrain	42±3	3.6±1.2	2.8±0.1

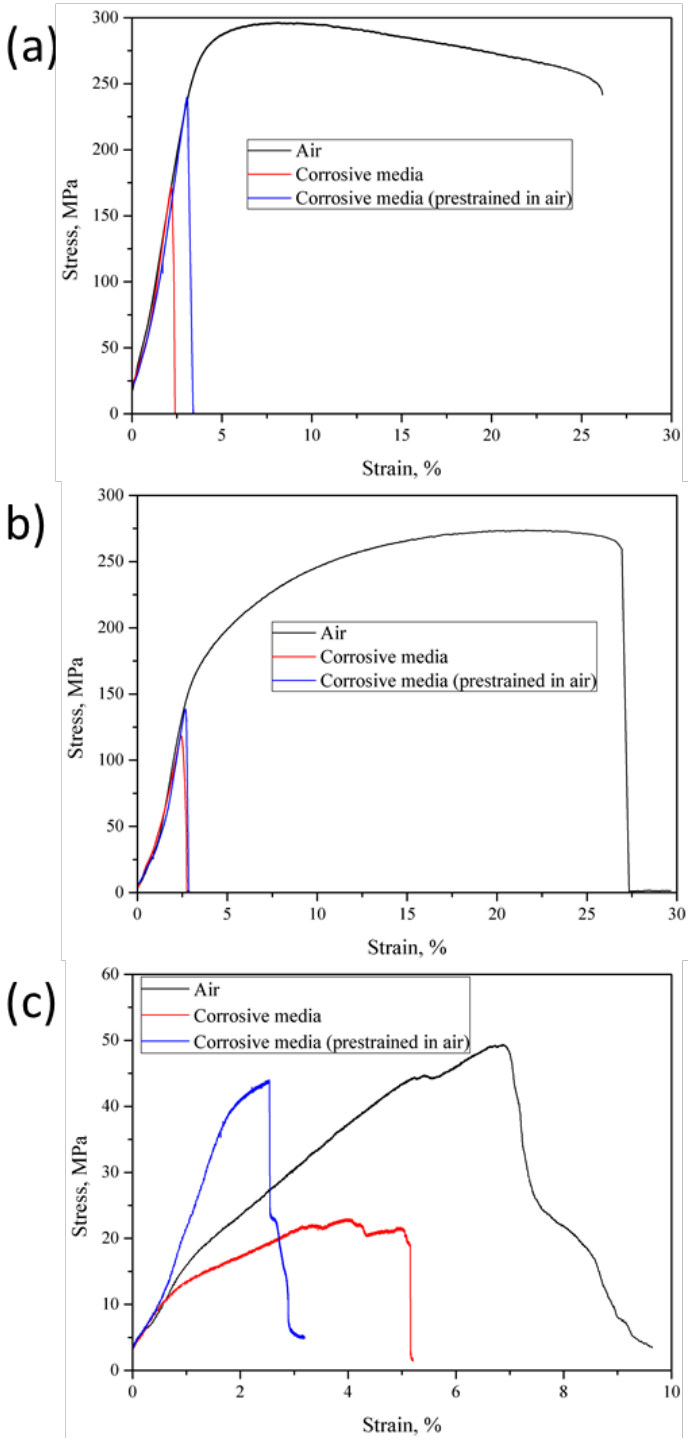

Fig. 2. The stress-strain diagrams of the SSRT-tested specimens of ZK60 (a), AZ31 alloys (b) and pure Mg (c).

3.3. Side surface analysis

The examination of the side surfaces of the specimens, which were exposed to corrosive media during SSRT tests, revealed different responses of the tested alloys to the same corrosion solution, Fig. 3. After testing, the surface of the ZK60 alloy was almost completely covered by the dense shell of dark corrosion products. Interestingly that the prestrained ZK60 specimens

show less severe corrosion damage in comparison with their as-received counterparts, Fig. 3b. Among the others, the alloy AZ31 exhibits the least corrosion damage, the extent of which is not influenced by prestraining. As could be seen in Fig. 3c, d, only a few dark corroded spots are found on the specimens of this alloy before and after prestraining. Figure 3e shows that the surface of the pure magnesium specimens, which were not prestrained before testing, demonstrates moderate corrosion damage, which is found less severe than that in the alloy ZK60 and more severe than that in AZ31, respectively. After prestraining, some specimens of pure Mg demonstrate the same extent of corrosion damage as the as-received ones, while others show notably less corrosion, c.f. Fig. 3f.

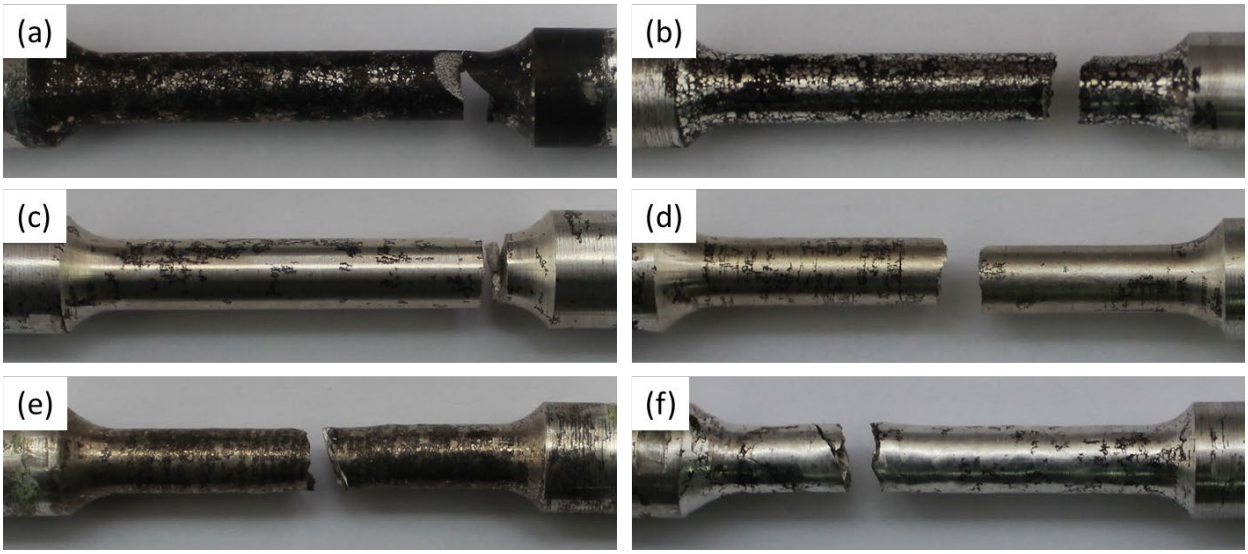

Fig. 3 – Gauge parts of alloys ZK60 (a, b), AZ31 (c, d) and as-cast pure Mg (e, f) SSRT tested in corrosive media: (a, c, e) as-received specimens and (b, d, f) prestrained specimens

3.4. Fractography

After testing in air, all specimens exhibit ductile fracture characteristics with typical dimple morphologies on the fracture surface, Fig. 4a-c. Pure Mg mainly demonstrates the so called fluted fracture surface relief with tubular voids, which typically nucleate at intersections of basal and non-basal slip planes [15], Fig. 4c.

The fracture surface of the ZK60 and AZ31 specimens failed in corrosive media exhibits primarily brittle regions with mixed trans-/intergranular appearance, Fig. 4d, e, g, h. The transgranular cleavage-like morphology predominates in the ZK60 alloy, while the AZ31 alloy shows stronger propensity to intergranular fracture. For both alloys, the brittle regions originate at the specimens surface, and are gradually transformed into a ductile relief on the way from the

side surface to the bulk. Similar fracture surface features are found in the prestrained specimens of the alloys, Fig. 4g, h.

The fracture surface of pure Mg tested in corrosive media is completely different from that of the alloys suffering SCC. It has the fluted morphology, Fig. 4f, similar to that of the specimens tested in air. However, in the case of specimens tested in corrosive environment, the flutes have smoother appearance with no or little amount of dimples and tear ridges on it. After prestraining followed by testing in corrosive media, the flutes on the fracture surface of pure Mg appear more ductile than in the specimens fractured due to SCC without prestraining, Fig. 4i, though it still seems to be less ductile in comparison with the specimens tested in air.

It should be noted, that even though the discussed fractography images are quite representative for all specimens tested, they do not comprehensively disclose multiple features of the evolving SCC fracture in Mg alloys. This will be considered in detail in the forthcoming companion paper dedicated specifically to fractographic analysis of Mg alloys failed due to SCC.

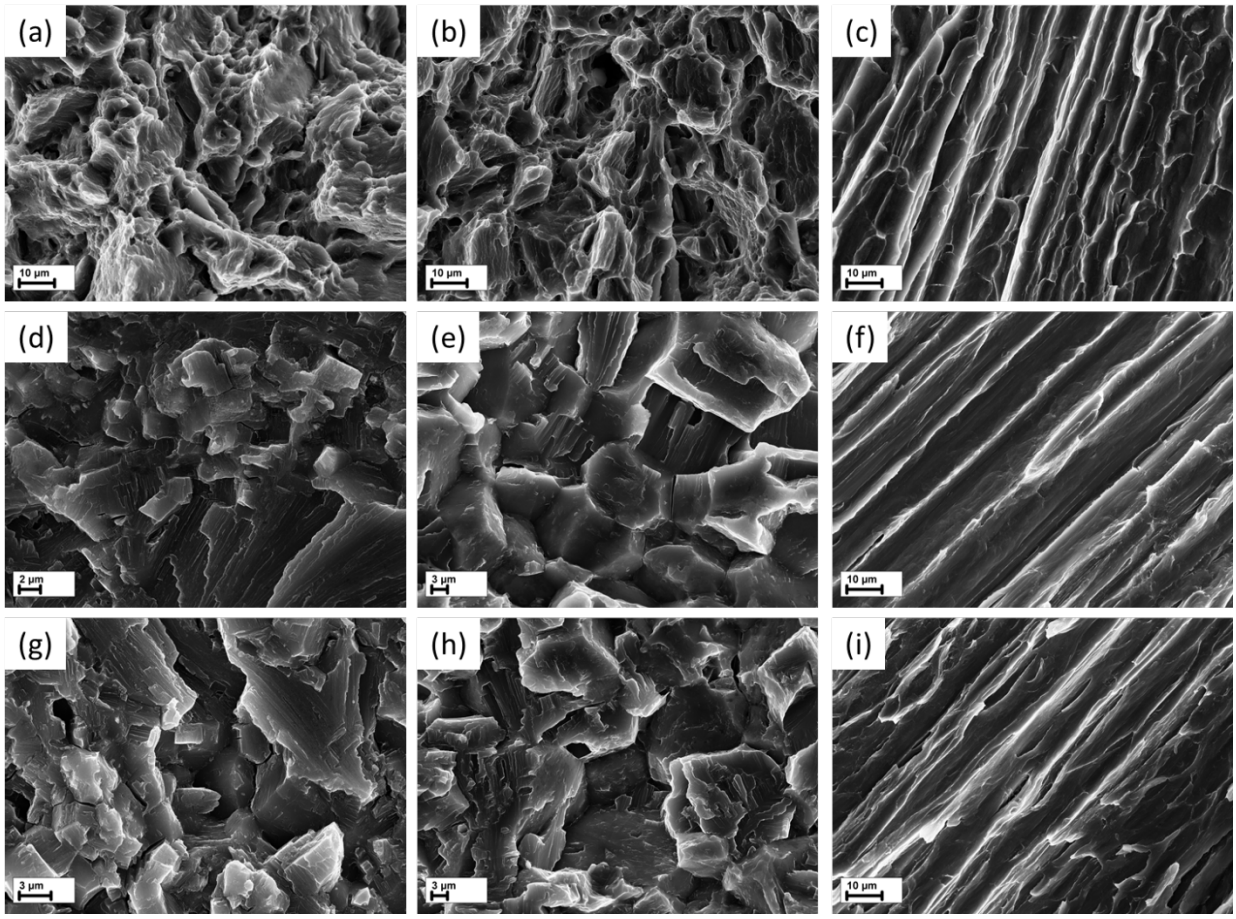

Fig. 4. Characteristic regions of the fracture surfaces of ZK60 (a, d, g), AZ31 (b, e, h) and pure Mg (c, f, i) tested in air (a-c) and in corrosive media (d-i), before (a-f) and after prestraining (g-i).

3.5. Gas analysis

The gas-analysis of the reference specimens of all alloys, which did not contact with corrosive media, showed no detectable hydrogen extraction in the temperature range from 25 to 450 °C. Figure 5 shows that after SSRT testing all specimens demonstrate the significant increase of hydrogen concentration, which was found to be the highest for the alloy ZK60. The main corrosion product, which is also known as the principal component of passive films in magnesium, is Mg hydroxide. Therefore, after removing corrosion products, the hydrogen concentration drops from 15.9 to 3.6 ppm for ZK60, from 10.6 to 7.3 ppm for pure Mg and from 10.5 to 5.2 ppm for the AZ31 alloy. It is worth to note that in the case of prestrained pure Mg the large scattering of hydrogen concentration is observed, c.f. Fig.5c. This is probably connected with the different extent of corrosion damage in these specimens, as was mentioned above.

The effect of preliminary straining on hydrogen concentration is found different depending on the material, and this effect is rather weak. The slightly higher hydrogen concentrations were found in the prestrained specimens of AZ31 alloy and pure Mg when the corrosion products were removed from their surface. In the case when the corrosion products retain on the surface, the hydrogen concentration is the same within the regular scatter for the prestrained and as-received specimens. Let us notice that prestraining results in the reduction of hydrogen concentration in the alloy ZK60, though after removing corrosion products this effect is less considerable.

As can be concluded from the extraction curves presented in Fig. 6, desorption of hydrogen from all specimens covered with corrosion products occurs in the whole temperature range from 25 to 450 °C. Conventionally, the extraction curves can be divided into low- and high-temperature parts with the approximate boundary between them at around 300 °C indicated by the dashed line in Fig. 6. For all the alloys, the greatest amount of hydrogen is extracted in the high-temperature range as pointed out by the pronounced peaks on the extraction curves. The desorption is continued even during the subsequent holding at 450 °C until the heater is turned off and the desorption rate is decreased down to the background level. Extraction curves of the specimens containing corrosion products are composed of several overlapping peaks, which number, heights and occurrence with respect to temperature vary to some extent depending on the alloy.

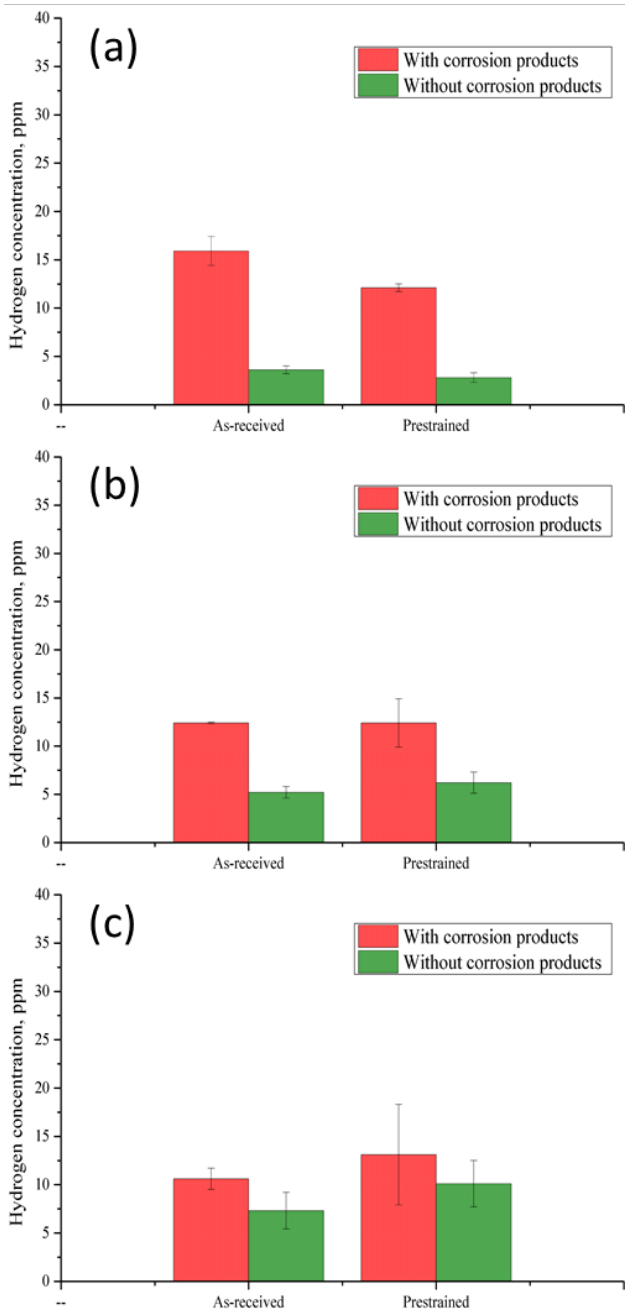

Fig. 5. Hydrogen concentration in SSRT tested specimens of ZK60 (a), AZ31 (b) alloys and pure Mg (c).

At temperatures below 300 °C, the most intensive desorption of hydrogen occurs in the alloy ZK60 where the desorption process is represented by at least three overlapping peaks, c.f. Fig. 6a, b. In the same temperature range, pure Mg exhibits only one pronounced peak, see Fig. 6e, f, while for the AZ31 alloy the release of hydrogen is too weak to distinguish between individual peaks, Fig. 6c, d. For all the alloys tested, the low-temperature part of extraction curves is almost not influenced by prestraining.

The high-temperature part of extraction curves for all alloys is composed of a few overlapping peaks. The highest peak appears at 440 °C for ZK60 alloy and at higher

temperatures for pure Mg and AZ31 alloy. Prestraining results in the reduction of the high-temperature peaks in the ZK60 alloy but it does not influence the peaks of the alloy AZ31; the only slight increase of hydrogen extraction peaks is observed in pure Mg.

It is important to notice that for all materials, removing corrosion products results in the complete vanishing of the low-temperature part of the extraction curves and in the substantial reduction of the height of high-temperature peaks. Thus, the desorption of hydrogen after removing corrosion products begins only at 280-300 °C and reaches its maximum rate at about 440 °C.

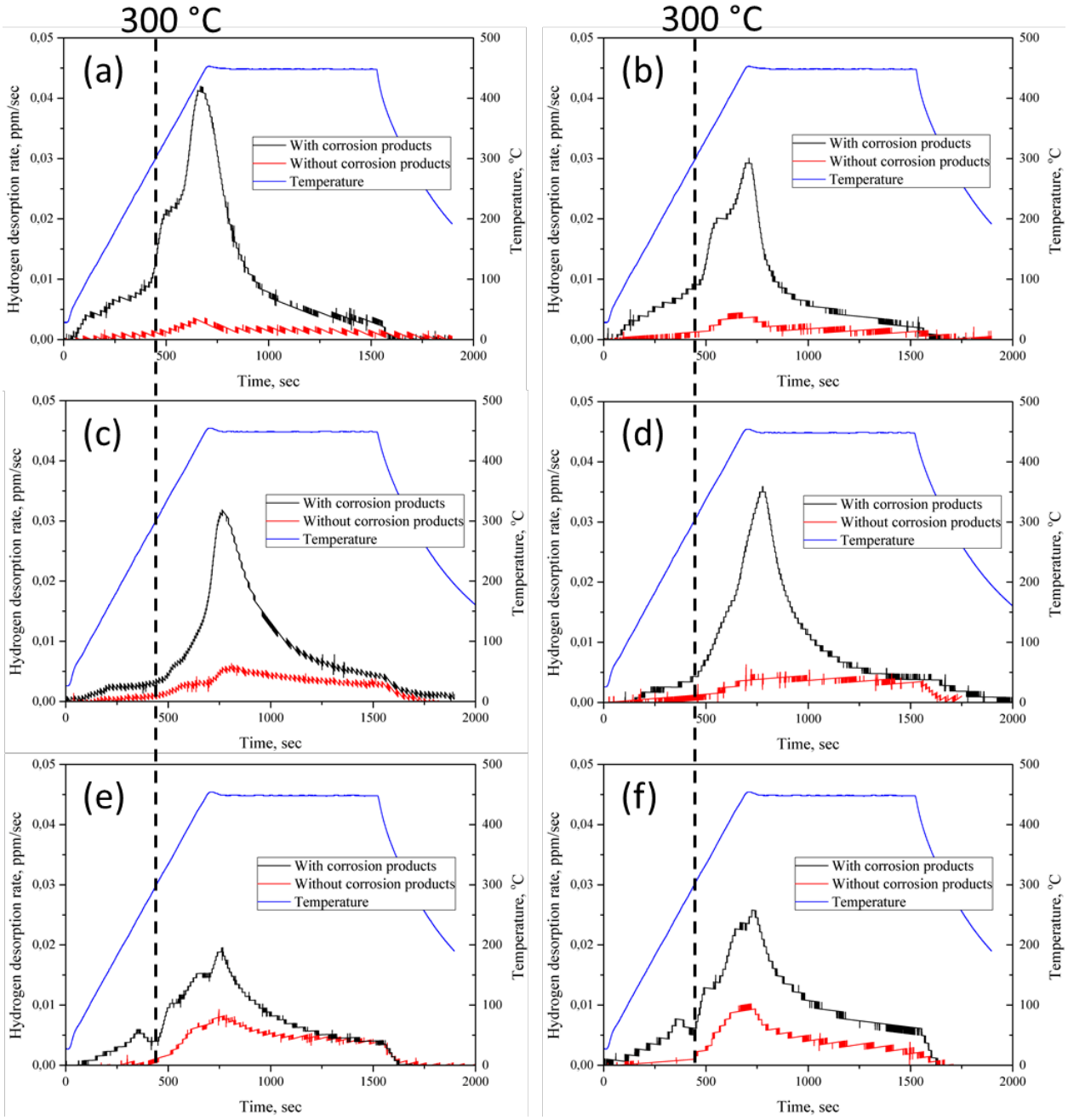

Fig. 6. Hydrogen extraction curves for SSRT-tested specimens of ZK60 (a), AZ31 (b) alloys and pure Mg (c) before (a, c, d) and after (b, d, f) prestraining.

4. Discussion

4.1. Sources of hydrogen desorbing below 300 °C

The results of the gas analysis strongly suggest that hydrogen extracting at the temperatures below 300 °C is predominantly contained in the surface layer of the specimens. Thus the following sources of hydrogen can possibly impact into the low-temperature part of extraction curves of the as tested specimens (before removal of corrosion products): (1) the decomposition of corrosion products, (2) the chemical reaction of Mg with the rest of corrosive media occurring on the specimen surface and (3) the desorption of diffusible hydrogen dissolved in the matrix surface layer, which can be further accidentally etched by the remover of corrosion products. The depth of the latter layer, however, does not exceed ~15 nm, as has been shown in the experimental part of the present study. In steels, diffusible hydrogen is commonly determined as that extracting from a specimen at the temperature below 300 °C [20]. This hydrogen, being very mobile at room temperature, is considered to quickly redistribute in the metal matrix and to affect the crack growth process. Diffusible hydrogen includes atomic hydrogen dissolved in the lattice and hydrogen reversibly trapped at the crystal lattice sites with the binding lattice energy lowered by the defects such as dislocations, grain boundaries, etc. [21–25]. It is generally established that the increase in the dislocations density in steels results in the considerable increase of diffusible hydrogen concentration [26]. It has been shown above that plastic prestraining, which is inevitably accompanied by the increase in the dislocation density, does not actually result in the increase of the concentration of hydrogen extracting below 300 °C for all investigated Mg-based materials. Hence, although the extraction curves reveal the desorption kinetics of hydrogen in the temperature range below 300 °C, it is unlikely that this process can be associated with diffusible hydrogen.

When the specimens of the ZK60 alloy completely covered by corrosion products were immersed in CCl_4 prior to gas-analysis, the streams of gas bubbles emanating from the specimens surface have been observed. The bubbles were not observed after removing corrosion products. Perhaps, at the beginning of the gas-analysis some corrosion reaction accompanying by evolution of hydrogen still occurred on the specimens surface. Therefore, it is concluded that the peak, appearing at the lowest temperature on the extraction curve of the alloy ZK60, is attributed to hydrogen produced by corrosion reaction occurring on the specimen surface.

Although the origin of other low-temperature desorption peaks on extraction curves have yet to be clarified in many details, it is apparent that most part of hydrogen desorbing below 300 °C range is associated with the decomposition of corrosion products deposited on the surface of

the specimen. This conclusion is corroborated by a number of experimental observations, which include the followings: (1) after removing corrosion products, no detectable desorption of hydrogen is found below 300 °C; (2) the area of low-temperature part of the extraction curves qualitatively correlates with the amount of corrosion products on the specimens surface; (3) the shape and area of the low-temperature part of the extraction curves for a given material is the same regardless of prestraining but is varied for different materials. The origin of this part of extraction curves will be clarified in the forthcoming publications.

4.2. Sources of hydrogen desorbing above 300 °C

Hydrogen evolving from the metal above 300 °C is commonly believed to be unable to move fast enough because it is irreversibly trapped or chemically bonded. Thus, the high-temperature desorption peaks appearing on the extracting curves can be attributed to the irreversibly trapped hydrogen or to the hydrogen stored in chemical compounds. As it is shown in Fig. 6 the removing corrosion products results in substantial reduction of hydrogen amount desorbing at temperature above 300 °C, particularly for ZK60 and AZ31 alloys. Thus, the considered high-temperature peaks are rather related to some chemical compounds, e.g. the Mg hydride, or the Mg hydroxide, or both, which are formed during exposure of the Mg's surface to corrosive media. According to the literature data, the hydroxide decomposes into the magnesium oxide (MgO) and hydrogen gas above 440 °C [8], which may correspond to the observed extraction peak. The decomposition temperature of the magnesium hydride can vary. The theoretical calculations show that the Mg hydride decomposes at temperatures above 281.9 °C [6]. According to this work and references therein, the decomposition temperature of the magnesium hydride experimentally measured by DSC was found to be 250 - 284 °C for milled and 438 °C for unmilled magnesium hydride. Evard et al. [27] using the thermal desorption analysis found that MgH_2 powder decomposed in the temperature range from 400 to 500 °C depending on heating rates whereas the partially hydrogenated magnesium MgH_x decomposed in the temperature range from 300 to 450 °C. Thereby, the decomposition temperature of magnesium hydride matches reasonably the temperature range of the high-temperature extraction peaks observed in the present study.

The presence of Mg hydride and hydroxide on the surface of investigated materials subjected to SSRT tests in corrosive media is quite reasonable. Perrault [28] showed that MgH_2 and $Mg(OH)_2$ are stable phases in Mg contacting with aqueous solutions. $Mg(OH)_2$, serving as protective film, is usually deposited on the Mg surface during the contact with water as has been observed by many investigators [6,29]. It also can be formed as the product of decomposition

MgH_2, if the latter is present [8]. Although the presence of MgH_2 in corroded Mg is usually less obvious than $Mg(OH)_2$, several authors have observed it. For example, Gulbrandsen [30] has found the X-ray diffraction lines corresponding to MgH_2 in corroded pure Mg. With the use of SIMS Chen et al. [6] observed MgH_2 in β-phase particles of AZ91 alloy exposed to the 0.1 M Na_2SO_4 solution for various times at free corrosion potential. Using the time-of-flight-secondary ion mass spectrometry (ToF-SIMS) Seyeux et al. [29] found MgH_2 in the thin 25 nm surface film of corrosion products on the surface of pure Mg immersed into ultrapure water for just 2 min. As was shown in the present study, removing corrosion products by 20% CrO_3+1%$AgNO_3$ solution results in the significant reduction of the height and area of the extraction curves above 300 °C for all the materials studied. It can be probably connected with the dissolution of $Mg(OH)_2$ or MgH_2 deposited on the surface of the specimen. Since the high-temperature desorption peaks appearing on the extraction curves before and after removing corrosion products have approximately the same position with respect to the temperature, their nature is likely similar. Thus presumably the high-temperature desorption peaks corresponding to the specimens with removed corrosion products is also caused by the decomposition of the retained part of MgH_2 and $Mg(OH)_2$, which are perhaps precipitated deeper in the Mg matrix or at the surfaces with restricted access for the CrO_3+1%$AgNO_3$ solution. The decrease of hydrogen concentration and height of the high-temperature desorption peak after removal of corrosion products from the pure Mg is less significant than for the ZK60 and AZ31. The reason for that can be probably associated with deeper hydride or hydroxide layer in pure Mg because of its larger grains.

4.3. The role of hydrogen in SCC

The aforementioned results of gas-analysis surprisingly showed that the concentration of diffusible hydrogen in the bulk as well as within the surface layer of as-received and prestrained specimens is negligible during SSRT testing in corrosive media. This observation indicates the only minor role of diffusible hydrogen and consequently less importance of the HEDE and HELP mechanisms in the SCC of Mg and its alloys. It is in contrast with the HE of steels, in which diffusible hydrogen is generally considered as the key factor controlling HAC [17]. The SCC of Mg can be probably attributed to DHC and AIDE, requiring the presence of hydrides and adsorbed hydrogen, respectively. It is believed that the fracture surface produced by the DHC mechanism should have brittle cleavage-like trans- or intergranular appearance, and that is exactly what is found in the ZK60 and AZ31 alloys, Fig. 4d, e, g, h. As has been shown above, hydrides are found by many investigators in corroded Mg and are the probable source of hydrogen desorbing at the temperatures above 300 °C in the present study. Thus the following

scenario for HAC of ZK60 and AZ31 alloys can be proposed. At first, the contact of Mg surface with corrosive media results in the quick formation of corrosion products film containing MgH_2 and $Mg(OH)_2$. Seyeux et al. [29] found the presence of MgH_2 and $Mg(OH)_2$ on Mg surface after 2 min immersion in water. This film is impermeable to diffusible hydrogen because of the extremely low diffusion coefficient of hydrogen in MgH_2 and $Mg(OH)_2$ [8]. The Cl^- anions cause the breakdown of protective $Mg(OH)_2$ film and provide access for hydrogen atoms to Mg surface. However, this hydrogen is probably consumed for the formation of Mg hydride, so the diffusible hydrogen does not penetrate deep into the bulk of a specimen, and its concentration in the matrix remains low. The increasing load during SSRT testing results in brittle fracture of surface hydrides. Once the hydride is cracked and the corrosion solution reaches the free Mg surface, the new hydride is formed. Thereby, the SCC occurs by alternating formation and fracture of the hydride surface film. Hypothetically, the fracture of MgH_2 occurs at a certain threshold stress. In the case of high-strength ZK60 and AZ31 alloys, this stress is probably achieved at the elastic stage of the stress-strain diagram.

The as-cast pure Mg has the very low yield stress and the ultimate tensile strength, which are likely less than the fracture stress of hydrides. The latter exerts therefore little effect on mechanical properties and the stress-strain diagram of pure Mg. The minor role of hydrides in SCC of pure Mg is also supported by fractographic data. As has been discussed above, the effect of corrosive media during SSRT testing on fracture surface of pure Mg is quite different in comparison with the alloys tested. In the case of pure Mg, the fracture surface appearance does not change completely due to SCC. Instead, after testing in corrosive media the fluted morphology of fracture surface in pure Mg becomes smoother and exhibits less ductile features such as dimples or tear ridges, than it does after testing in air. This observation is exactly the same to that found by Lynch and Trevena in [15]. They concluded that SCC of Mg occurred by a more localized microvoid-coalescence process than that in inert environments. Such a behavior was explained through the AIDE mechanism implying that hydrogen adsorbing on a crack's surface reduces the surface energy and promotes dislocation emission from the crack tip. As can be seen in Fig. 2c, the strain hardening of pure Mg in corrosive media occurs at the lower flow stress than in air. This is indicative of the reduced stress required for dislocation motion due to hydrogen adsorption on the specimen's surface. Taking into account the mechanical behavior and fractographic features of pure Mg subjected to SCC as well as the fact that the AIDE does not require the presence of diffusible hydrogen, it can be suggested that the SCC of pure Mg is associated with the AIDE mechanism.

It should be noted that, besides the DHC and AIDE, the SCC can also be promoted to some extent by the anodic dissolution mechanism. Particularly, it can be responsible for the crack

initiation at the specimen's side surface. However, additional study is needed to gain a better understanding of the role of DHC, AIDE and AD mechanisms and their interplay.

4.4. The effect of prestraining on SCC

It is found that prestraining exerts an ambiguous effect on susceptibility of Mg and its alloys to SCC. The specimens of ZK60 and AZ31 show slightly higher mechanical properties in corrosive media after prestraining, while prestrained as-cast pure Mg demonstrates the lower elongation at failure but higher ultimate tensile strength in corrosive media in comparison with the as-received state. This result is again in contrast with the behavior of hydrogen embrittled or SCC-tested steels which commonly demonstrate the substantial decrease of mechanical properties after prestraining. This effect is commonly explained by the increase of diffusible hydrogen concentration, which in turn is caused, by the increase of dislocations density. As was shown in the present study, prestraining does not result in the increase of hydrogen concentration in Mg and its alloys. Moreover, in the ZK60 alloy, it results in the decrease of hydrogen concentration as can be seen from the reduction of the high-temperature desorption peaks. It can be supposed that the formation of hydrides is more difficult in the prestrained specimens because of residual stresses at the surface. This also can explain the slightly higher mechanical properties of ZK60 and AZ31 alloys in corrosive media after prestraining. Indeed, if the SCC of an alloy is associated with brittle fracture of hydrides, than the stress at fracture should be mainly determined by the fracture stress of hydrides and their amount. Thus, if prestraining does not significantly affect the amount of hydrides, the stress at fracture of a specimen of the alloy should not strongly depend on the amount of the preliminary imposed plastic strain. As has been discussed above, the mechanism of SCC of pure Mg is different from that of the alloys and is associated rather with AIDE than with DHC. Therefore, the different influence of prestraining on SCC in Mg is not surprising. The yield stress of pure Mg increases due to strain hardening. At the higher stress, the crack growth facilitated by the AIDE mechanism may occur faster. Consequently, the fracture of prestrained pure Mg is observed at lower strain and at higher stress.

5. Conclusions

1. The desorption of hydrogen from pure Mg and Mg alloys SSRT tested in corrosive media is not associated with the extraction of diffusible hydrogen absorbed by Mg matrix but is likely related to the decomposition of corrosion products.

2. The decomposition of magnesium hydride and hydroxide is a most probable source of hydrogen desorbing from pure Mg, ZK60 and AZ31 alloys subjected to SCC in the temperature range from 300 to 450 ˚C.

3. The concentration of diffusible hydrogen in pure Mg, ZK60 and AZ31 alloys after several hours of SSRT testing in 5 g/l NaCl + 5 g/l $K_2Cr_2O_7$ is negligible. Thereby the role of diffusible hydrogen in the mechanism of SCC of Mg and its alloys should be relatively insignificant.

4. The as-cast pure Mg has much lower susceptibility to SCC in comparison with wrought ZK60 and AZ31 alloys. In contrast to the alloys, fractured at quasi-elastic strain region, the pure Mg demonstrates appreciable plastic straining during SSRT-testing in corrosive 5 g/l NaCl + 5 g/l $K_2Cr_2O_7$ media.

5. Preliminary plastic straining results in the increase of mechanical properties of the alloys ZK60 and AZ31 when they are SSRT tested in the corrosive solution, while prestrained as-cast pure Mg demonstrates the lower strain at fracture but the higher ultimate tensile strength. Nevertheless, the observed effects of prestraining on the mechanical properties and hydrogen concentration are found to be rather small.

6. The SCC of ZK60 and AZ31 alloys is accompanied by formation of mixed trans-/intergranular brittle fracture surface. However, the ZK60 alloy is mostly prone to transgranular cleavage-like cracking, while AZ31 shows stronger propensity to brittle intergranular fracture. The fracture mode of pure Mg at SSRT testing changes (but does not alter completely) when the testing environment changes from air to the corrosive solution: the surface of flutes on the fracture surface of pure Mg becomes smoother due to reduction of dimples.

7. The SCC mechanism of ZK60 and AZ31 is different from that of pure Mg. The SCC of ZK60 and AZ31 alloys is likely associated with delayed-hydride cracking, while the SCC of pure Mg can be explained by adsorption-induced dislocation emission theory.

6. Acknowledgements

Financial support from the Russian Science Foundation through the grant-in-aid No. 18-19-00592 is gratefully appreciated.

List of References

[1] K.W. Guo, A Review of Magnesium/Magnesium Alloys Corrosion and its Protection, Recent Patents Corros. Sci. 2 (2010) 13–21. doi:10.2174/1877610801002010013.

[2] A. Atrens, W. Dietzel, P. Bala Srinivasan, N. Winzer, M. Bobby Kannan, Stress corrosion

cracking (SCC) of magnesium alloys, in: Stress Corros. Crack., Elsevier, 2011: pp. 341–380. doi:10.1533/9780857093769.3.341.

[3] A. Atrens, N. Winzer, W. Dietzel, Stress corrosion cracking of magnesium alloys, Adv. Eng. Mater. 13 (2011) 11–18. doi:10.1002/adem.200900287.

[4] D.G. Chakrapani, E.N. Pugh, Hydrogen embrittlement in a Mg-Al alloy, Metall. Trans. A. 7 (1976) 173–178. doi:10.1007/BF02644454.

[5] F. Tuchscheerer, L. Krüger, Hydrogen-induced embrittlement of fine-grained twin-roll cast AZ31 in distilled water and NaCl solutions, J. Mater. Sci. 50 (2015) 5104–5113. doi:10.1007/s10853-015-9064-3.

[6] J. Chen, J. Wang, E. Han, J. Dong, W. Ke, States and transport of hydrogen in the corrosion process of an AZ91 magnesium alloy in aqueous solution, Corros. Sci. 50 (2008) 1292–1305. doi:10.1016/j.corsci.2008.01.028.

[7] X. He, Z. Yan, H. Liang, Y. Wei, Study on Corrosion and Stress Corrosion Cracking Behaviors of AZ31 Alloy in Sodium Sulfate Solution, J. Mater. Eng. Perform. 26 (2017) 2226–2236. doi:10.1007/s11665-017-2644-4.

[8] M. Kappes, M. Iannuzzi, R.M. Carranza, Hydrogen Embrittlement of Magnesium and Magnesium Alloys: A Review, J. Electrochem. Soc. 160 (2013) C168–C178. doi:10.1149/2.023304jes.

[9] R.S. Stampella, R.P.M. Procter, V. Ashworth, Environmentally-induced cracking of magnesium, Corros. Sci. 24 (1984) 325–337. doi:10.1016/0010-938X(84)90017-9.

[10] N. Winzer, A. Atrens, G. Song, E. Ghali, W. Dietzel, K.U. Kainer, et al., A critical review of the Stress Corrosion Cracking (SCC) of magnesium alloys, Adv. Eng. Mater. 7 (2005) 659–693. doi:10.1002/adem.200500071.

[11] N. Winzer, A. Atrens, W. Dietzel, G. Song, K.U. Kainer, Evaluation of the delayed hydride cracking mechanism for transgranular stress corrosion cracking of magnesium alloys, Mater. Sci. Eng. A. 466 (2007) 18–31. doi:10.1016/j.msea.2007.03.020.

[12] N. Winzer, A. Atrens, W. Dietzel, V.S. Raja, G. Song, K.U. Kainer, Characterisation of stress corrosion cracking (SCC) of Mg – Al alloys, Mater. Sci. Eng. A. 48 (2008) 339–351.

[13] N. Winzer, A. Atrens, W. Dietzel, G. Song, K.U. Kainer, Fractography of stress corrosion cracking of Mg-Al alloys, Metall. Mater. Trans. A Phys. Metall. Mater. Sci. 39 A (2008) 1157–1173. doi:10.1007/s11661-008-9475-8.

[14] L.F. Zhou, Z.Y. Liu, W. Wu, X.G. Li, C.W. Du, B. Jiang, Stress corrosion cracking behavior of ZK60 magnesium alloy under different conditions, Int. J. Hydrogen Energy. 42 (2017) 26162–26174. doi:10.1016/j.ijhydene.2017.08.161.

[15] S.P. Lynch, P. Trevena, Stress corrosion cracking and liquid metal embrittlement in pure magnesium, Corrosion. 44 (1988) 113–124.

[16] S.P. Lynch, Hydrogen embrittlement phenomena and mechanisms, Corros. Rev. 30 (2012) 63–133. doi:10.1515/corrrev-2012-0502.

[17] I.M. Robertson, P. Sofronis, A. Nagao, M.L. Martin, S. Wang, D.W. Gross, et al., Hydrogen Embrittlement Understood, Metall. Mater. Trans. A. 46 (2015) 2323–2341. doi:10.1007/s11661-015-2836-1.

[18] M. Nagumo, Fundamentals of Hydrogen Embrittlement, Springer Singapore, Singapore, 2016. doi:10.1007/978-981-10-0161-1.

[19] G.I. Morozova, Phase composition and corrosion resistance of magnesium alloys, Met. Sci. Heat Treat. 50 (2008) 100–104. doi:10.1007/s11041-008-9020-9.

[20] A. Laureys, T. Depover, R. Petrov, K. Verbeken, Influence of sample geometry and microstructure on the hydrogen induced cracking characteristics under uniaxial load, Mater. Sci. Eng. A. 690 (2017) 88–95. doi:10.1016/j.msea.2017.02.094.

[21] K. Ono, M. Meshii, Hydrogen detrapping from grain boundaries and dislocations in high purity iron, Acta Metall. Mater. 40 (1992) 1357–1364. doi:10.1016/0956-7151(92)90436-I.

[22] J.Y. Lee, J.L. Lee, A trapping theory of hydrogen in pure iron, Philos. Mag. A. 56 (1987) 293–309. doi:10.1080/01418618708214387.

[23] F. Wei, T. Hara, K. Tsuzaki, Precise determination of the activation energy for desorption of hydrogen in two Ti-added steels by a single thermal-desorption spectrum, Metall. Mater. Trans. B. 35 (2004) 587–597. doi:10.1007/s11663-004-0057-x.

[24] L. Cai, L. Zhao, Effect of hydrogen trapping and poisons on diffusion behavior of hydrogen in low carbon steel, Key Eng. Mater. 764 (2018) 3–10. doi:10.4028/www.scientific.net/KEM.764.3.

[25] M. Kamilyan, R. Silverstein, D. Eliezer, Hydrogen trapping and hydrogen embrittlement of Mg alloys, J. Mater. Sci. 52 (2017) 11091–11100. doi:10.1007/s10853-017-1268-2.

[26] W.Y. Choo, J. Lee, Thermal analysis of trapped hydrogen in pure iron, Metall. Trans. A. 13 (1982) 135–140. doi:10.1007/BF02642424.

[27] E.A. Evard, I.E. Gabis, M.A. Murzinova, Kinetics of hydrogen liberation from stoichiometric and nonstoichiometric magnesium hydride, Mater. Sci. 43 (2007) 620–633. doi:10.1007/s11003-008-9002-5.

[28] G.G. Perrault, The potential-pH diagram of the magnesium-water system, J. Electroanal. Chem. Interfacial Electrochem. 51 (1974) 107–119. doi:10.1016/S0022-0728(74)80298-6.

[29] A. Seyeux, M. Liu, P. Schmutz, G. Song, A. Atrens, P. Marcus, ToF-SIMS depth profile of

the surface film on pure magnesium formed by immersion in pure water and the identification of magnesium hydride, Corros. Sci. 51 (2009) 1883–1886. doi:10.1016/j.corsci.2009.06.002.

[30] E. Gulbrandsen, Anodic behaviour of Mg in HCO− 3/CO 2− 3 buffer solutions. Quasi-steady measurements, Electrochim. Acta. (1992) 1403–1412. http://www.sciencedirect.com/science/article/pii/001346869287014Q.